

# Photocrystallography

Jacqueline M. Cole

Cavendish Laboratory, University of Cambridge, J. J. Thomson Avenue, Cambridge, CB3 0HE, UK.  
Correspondence e-mail: jmc61@cam.ac.uk

This review describes the development and application of a new crystallographic technique that is starting to enable the three-dimensional structural determination of molecules in their photo-activated states. So called 'photocrystallography' has wide applicability, particularly in the currently exciting area of photonics, and a discussion of this applied potential is put into context in this article. Studies are classified into four groups: photo-structural changes that are (i) irreversible; (ii) long-lived but reversible under certain conditions; (iii) transient with photo-active lifetimes of the order of microseconds; (iv) very short lived, existing at the nanosecond or even picosecond level. As photo-structural changes relative to the 'ground state' can be subtle, this article necessarily concentrates on small-molecule single-crystal X-ray diffraction given that high atomic resolution is possible. That said, where it is pertinent, references are also made to related major advances in photo-induced macromolecular crystallography. The review concludes with an outlook on this new research area, including the future possibility of studying even more ephemeral, femtosecond-lived, photo-active species.

© 2008 International Union of Crystallography  
Printed in Singapore – all rights reserved

## 1. Introduction

Over the last few decades, the world has experienced an optical and electro-optical revolution: digital light displays that light up car dashboards, mobile phones and stereo sound systems; fluorescent and phosphorescent screens, for example in portable computers; underwater lighting equipment and night-working apparatus; optical switches and shock-wave triggers for use within electronic circuitry itself. The optoelectronic and photonics industry was estimated to be worth USD 236 million on the world market in 2004, and is expected to exceed USD 1 trillion by 2015 (Wallace, 2006). Consequently, there is a clear need for major research and development in this area, in order to better understand the underlying mechanisms from which such industrial applications emanate so that one can best exploit this knowledge *via* innovation.

It is generally known that the controlling optical and optoelectronic phenomena are all the result of electronic charge transfer or ionic displacement within a molecule. However, the details of such dynamics cannot be generalized for all materials since there is such a wide diversity of chemicals that exhibit these effects. Moreover, the precise nature of optical properties is frequently so subtle that optical effects can vary by orders of magnitude even within a series of compounds that have a major part of the chemical fragment in common. It is therefore vital to study in depth the molecular structure of optical and optoelectronic candidate materials, and establish relationships between the structure and the observed physical properties. Once one has built up sufficient

relationships, one can start to 'structurally engineer' materials to tailor them for a specific device application.

The structural characterization tools required for this work are based on X-ray and neutron diffraction, X-ray absorption spectroscopy, and infrared and optical spectroscopy. With a few exceptions, X-ray crystallography is generally regarded as the most practical and informative of these techniques. This is because X-ray facilities are more available and require only small samples. The sample size is particularly important since the optical source must be able to pass through the whole of the sample so that uniform photo-activation is realized. Generally speaking, the optical penetration depth of a sample increases from inorganic to organometallic to organic material types, and can range from just a few nanometres up to a few hundred micrometres in particularly favourable cases. Given this and the fact that the highest level of structural information comes from single-crystal diffraction, by some margin, this review concentrates on photocrystallographic research on single-crystal X-ray diffraction. However, references to key results obtained from other sources are included where appropriate to place the developing subject into a broader context.

## 2. Types of photo-active changes in compounds

The application of light to a material can promote electrons into 'excited states' if the light energy matches the energy gap between quantized low-lying energy levels of the material. This electronic excitation induces a redistribution of electrons

at the molecular level that can lead to atomic displacements within a solid material or, in more extreme cases, to isomerization or solid-state chemical reactions. Associated with these structural changes are a number of phenomena such as luminescence or radical formation.

This photo-activation can result in reversible or irreversible structural changes, and those that are reversible may be so only under certain environmental conditions (*e.g.* sample temperature, pressure, magnetic or photonic stimulus). Any photo-structural change will take a finite period of time to occur. For many materials, the photo-excited structure is ephemeral, perhaps existing for only a few microseconds or less. However, photo-activation can be much more long-lived; indeed, it can be metastable, *i.e.* infinitely long lived as long as the material remains under certain environmental conditions.

In this review, photo-induced processes are categorized into four types according to their different photonic applications: (i) irreversible structural changes that are relevant to optical etching and chemical reactions; reversible structural changes that (ii) are metastable (*e.g.* optical switches), (iii) have microsecond lifetimes (typically phosphorescent materials), (iv) exhibit nanosecond–picosecond-lived emissions (fluorescent species). Such applications are described in tandem with these time-related processes.

### 3. Considerations of molecular environment

Photo-excitation has been studied for many years using optical spectroscopy. However, results obtained from such experiments are indirect since they arise from samples that are usually in solution, whilst most materials-centred applications are in solid-state devices. In addition, solution measurements do not reveal any information about possible effects due to the crystal-lattice environment. Conversely, any effect of the solvent used in the solution is assumed to be negligible, whilst in practice the nature of the solvent can affect optical spectroscopy spectra considerably. The temperature at which an optical spectrum is obtained can also strongly affect the optical data since data are typically taken at room temperature and frozen nitrogen at 77 K, which represents data from the same sample in two phases: a low viscous solution and a glassy solvent matrix surrounding the frozen active medium. In addition to effects of sample phase, the optical phenomena themselves are frequently temperature dependent; for example, metal-to-ligand charge-transfer (MLCT) processes that are commonly observed in organometallic complexes often convert to an intra-ligand (IL) charge-transfer mechanism at liquid-nitrogen temperatures.

Furthermore, since the spectra from which one observes the physically changing phenomena in optical spectroscopy are often broad and somewhat featureless, or spectral profiles are lacking in distinct character, results are often interpreted indirectly *via* profile similarity with spectra from other compounds or *via* correlating experimental findings with computational predictions. In any case, such spectra can only generally provide qualitative information.

From the materials-centred perspective of solid-state device application, and in order to realize more simple, direct and quantitative results on photo-activated structural perturbations, it is therefore important to investigate solid-state to solid-state photo-structural effects. Those effects that occur in the single-crystal phase where the crystallographic lattice remains intact during this photo-excitation process provide the most informative results. Owing to lattice strain, one should note that one seldomly observes 100% photoexcitation; indeed, spin-crossover transitions are the one exception for reasons discussed later. Rather, one typically observes photostructural changes in up to 20% of unit cells.

The phase of the material under investigation is therefore critical to the interpretation of the results. Thus, when making comparisons between results from diffraction experiments, spectroscopy or even theoretical calculations, it is important to try, as far as it is possible, to obtain same phase comparisons.

### 4. The study of irreversible light-induced structural changes [type (i) materials]

#### 4.1. Optical etching and chemical reactions

Photo-induced chemical reactions are of course very important in their own right since they open up whole new areas of synthetic and mechanistic chemistry. Photo-activation usually acts to overcome the activation energy for a reaction to proceed. Depending on the nature of the chemical reaction and on the energetics involved, such a reaction may be reversible or irreversible. Either outcome is very useful for a number of optical applications, as one can optically etch a solid-state device that contains the photo-active chemical so as to record information either temporarily or permanently.

Such materials have particularly high potential as optical data storage media. Irreversible light-induced solid-state structural changes would suit write-once read-only data storage media, *i.e.* creating a permanent record of a set of information. The importance of using the most appropriate materials for optical storage cannot be understated, given its importance in computing and memory hardware. And yet there is a materials supply bottleneck in finding suitable materials, especially materials that can be used in future generation optical data storage.

In particular, there is presently immense commercial interest in developing holographic storage, hailed as the next-generation revolutionary storage media (Brinkman & Pinto, 1997). Holographic storage will allow threefold data encryption onto a single point, thus exploiting the volume of a material rather than just its surface area, as used on a compact disc (CD) or digital versatile disc (DVD), for example. Hologram memory can be created by focusing successive interference patterns of two light beams into a specific volume of a material. Each pattern relates to one page of data, coded as light and dark boxes on a screen, through which one of the incoming beams passes (the data-carrying beam). The two beams have been split from a single laser source and so the second beam, which passes through no screen, acts as a

reference signal (no data information) upon their coalescence. With the proposed ability to store over 100 times the data capacity of a DVD in material the size of a sugar cube (Fig. 1), the potential of this new media is incredible. However, developments are currently largely hampered by two factors. One problem lies in the stringent requirements of data retrieval: data is reconstructed by diffracting a further light beam, at the same angle as the reference beam enters the material, onto a detector; an error of one millionth of a metre will render the data irrecoverable. The other problem is that there is a dearth of suitable materials for long-lived device application. Given the high speed of industrial drive in this area, it is critical that materials chemistry keep up with the technological developments and it will only do so by understanding the structural manifestations of the light processes ensuing in the application. Inevitably, the optical etching created in the material needs to be as long lived as possible, else data will be lost irrecoverably over time. Therefore,



**Figure 1**

A photograph of 100 stacked DVDs and a sugar cube. If holographic storage achieves its expectation, one will be able to store a terabyte (1000 Gb) of data in a crystal the size of a sugar cube. Employing current commercial optical storage devices, a terabyte of data would fill more than 1000 compact discs, or over a 100 DVDs. The use of a sugar cube as a placebo here is a deliberate attempt to emphasize the fact that, although optical technology is developing rapidly, scientists are still struggling to find suitable materials for the application.

irreversible photo-active processes have enormous potential in this area.

#### 4.2. Experimental procedure

For materials undergoing irreversible photo-structural changes, conventional single-crystal diffraction methods are used. Firstly, one determines the non-photo-activated structure of the material by normal means. Then the crystal, still mounted on the X-ray diffractometer, is optically pumped for several hours with a suitable light source, typically either a flash lamp emitting light at wavelengths in a broad band or a laser (monochromatic source). The light source is then removed and the resulting photo-induced structure is determined under the otherwise same experimental conditions as were used for the non-photo-activated structure determination. In order to ensure reproducibility of measurements, automatic alignment facilities of light sources can be implemented (Thompson *et al.*, 2004). Following independent structural refinement of the two resulting sets of data, a straightforward 'before and after' structural comparison can be made, and the photo-structural effect thus identified and quantified. In some cases, data collections are also possible mid-way through a photo-structural change if this change is sufficiently slow or if the photo-structural change can be temporarily suspended, *e.g.* by freezing and trapping the sample. Where such structural inquiry is possible, one can obtain valuable information about the mechanism by which the complete structural change is obtained.

#### 4.3. Results obtained so far

The general outline of solid-state reactions has already been given by Schmidt and Cohen, McBride, Hammond and Zimmerman in the 1960s and 1970s (Cohen & Schmidt, 1964; McBride, 1983; Weiss *et al.*, 1993; Zimmerman *et al.*, 1998) whilst single-crystal to single-crystal photo-crystallographic application was pioneered by Nakanashi *et al.* (1980, 1981). Ohashi and co-workers have extended this area of research to various chemical reactions in molecular crystal systems. The impetus behind their work has been single-crystal to single-crystal photochemical reactions and an associated mechanistic enquiry of reaction intermediates. X-ray diffraction studies have concentrated on initial-state (before irradiation) and final-state (after irradiation) crystallography. Studies have involved proton transfer (Ohhara *et al.*, 2000), formation of a heterocyclic ring (Takayama *et al.*, 2003), asymmetry generation and chiral inversion (Sekine *et al.*, 1997), formation of a radical pair (Kawano *et al.*, 2002), ligand substitution in organometallic compounds (Sato *et al.*, 2007), excited-state formation (Kawano *et al.*, 2007). Separately, Kawano and co-workers have also described photochemical reactions that result in the formation of heterocyclic rings (Furusawa *et al.*, 2007), organometallic catenation (Yamashita *et al.*, 2007) and olefin dimerization (Takaoka *et al.*, 2006). Techert and co-workers have also reported the structure of photodimerization reactions (Davaasumbuu *et al.*, 2006). In a few cases, mechanistic information about reactions has also been illustrated

via isolation of the structure of the intermediate itself (Takayama *et al.*, 2003).

As an integral part of this work, the structural manifestations of some conformational changes have afforded useful insight into the topological nature of the reaction cavity in reaction types in a given series. In some cobaloxime complexes, for example, among Ohashi's featured compounds, the nature of reaction cavities has been probed by photoisomerization of cobaloxime complexes as guests within cyclohexylamine hosts (Hashizume & Ohashi, 1999).

Some of these photochemical reactions have been shown to be selectively reversible under certain conditions, although the possible reversibility greatly depends on the level of chemical or conformational change afforded in the photo-reaction, which might be substantial. For example, if the chemical change results in a large stabilization of lattice energy, reversibility is not likely. If a conformational change is too large, crystal fracture occurs as the crystal lattice can withstand molecular movement up to only a certain level before losing its integrity.

## 5. The study of metastable photo-activated structures [type (ii) materials]

### 5.1. Optical, thermo-optic and magneto-optic switches

Solid-state photo-induced structural changes can be metastable, which we define as infinitely long lived as long as they remain under suitable control (*e.g.* temperature, magnetic

field); outside this control, the structural change becomes reversible. By exploiting this control, one can switch between the photo-induced and non-photo-induced state at one's will. Alternatively, a photo-induced structure can be stable under ambient conditions until it is reversed by electromagnetic radiation (typically optical, UV or IR) of a wavelength different to the optical probe used in the original photo-activation.

Such optical switches are highly desirable in electronics and recording media since the reversible photo-structural change can represent binary information: 0 (original structure) and 1 (photo-activated structure). The reversibility means that associated devices can have read–write functionality.

The study of metastable photo-activated structures is therefore very important given its applicability to an eventual key functionality in industry.

### 5.2. Steady-state experimental methods

For materials exhibiting metastable photo-structural changes, the general experimental method is the same as that described for compounds exhibiting irreversible photo-structural changes (§4.2). Since no more than about 20% photo-conversion is obtained (see §3), the resulting structure from this second data collection comprises contributions from both the original ground state and the light-induced structure. In order to isolate the light-induced structure, analytical means are used. This requires first importing the refined ground-state structural model, obtained using the data from the first experimental step, into the 'ground plus light-induced' refinement model as a fixed entity, except that all atomic coordinates are normalized to the unit-cell parameters of the 'ground plus light-induced' state. The normalization is to take into account the slight change that is expected because of a small perturbation in the overall molecular environment from having two similar but not exact molecules present rather than one type. A new scale factor is then refined against the 'ground plus light-induced' data and a 'photodifference' map thence obtained: this map is essentially a Fourier-difference map that reveals the photo-induced structure exclusively because account of the ground-state structure has already been taken through the normalized fixed coordinates (see, for example, Fig. 2). The atomic positions of the photo-induced structure are therefore locatable from this map using standard procedures for interpreting Fourier-difference maps and are refined to produce the final combined ground-plus-photo-induced model. The occupancy factor of all atoms in each component should be refined as a common factor with both factors summing to 100% – exactly as one would model molecular disorder – so that one can realize the fraction of photo-conversion achieved: that value is the occupancy factor of the light-induced structure.

Steady-state methods rely on the light-induced effect in a single-crystal sample lasting for the duration of an X-ray diffraction data collection that is complete enough to achieve a full structural determination. Satisfying this condition depends critically on a number of factors: the rate at which

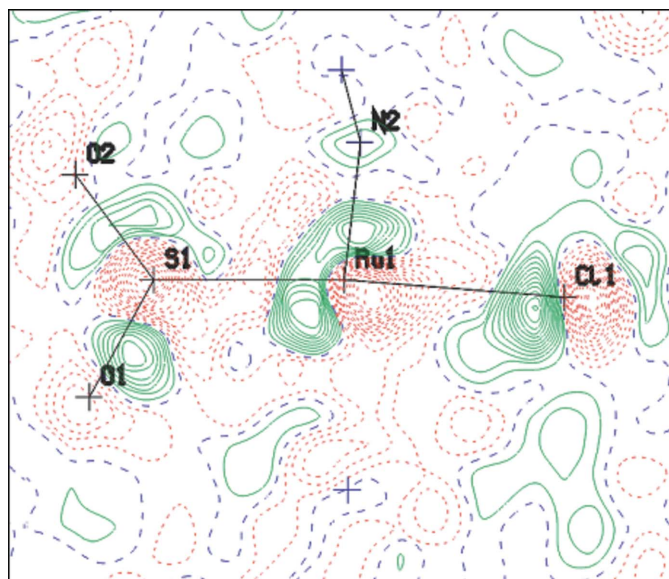


**Figure 2**

A 'photo-difference' map showing the ground state (already modelled) depicted by the black lines together with the electron density associated with the light-induced  $[\text{Ru}(\text{SO}_2)(\text{NH}_2)_4\text{Cl}]\text{Cl}$  complex (Kovalevsky *et al.*, 2002, 2003). In this example,  $\text{SO}_2$  is the photo-active ligand, undergoing an  $\eta^1$ - $\text{SO}_2$  (end-on) to  $\eta^2$ - $\text{SO}_2$  (side-bound) photoisomerization. The S atom and one O atom of the  $\eta^2$ - $\text{SO}_2$  bound ligand are evident in this Fourier-difference map as the green feature and more diffuse green area, respectively, on the left of the figure (the other O atom is not visible here as it lies outside the plane).

data can be collected; the crystal size of the sample; the intrinsic X-ray scattering strength, optical penetration depth and crystal symmetry of the subject material; wavelength, intensity and resolution of the X-ray source. For a favourable case, given current technology, one might estimate the minimum light-induced lifetime to be 20–30 min. For detailed consideration of these factors, the reader is referred to Cole (2004).

### 5.3. Steady-state photo-structural changes: results

The first reported crystallographic investigation in which *steady-state* photo-induced methods were applied involved a putative light-induced structural change in sodium nitroprusside (SNP),  $\text{Na}_2[\text{Fe}(\text{CN})_5(\text{NO})] \cdot 2\text{H}_2\text{O}$ , undertaken by Woike and co-workers (Rüdlinger *et al.*, 1991, 1992). Neutron diffraction was in fact used to reveal the structures of two metastable states,  $\text{MS}_\text{I}$  and  $\text{MS}_\text{II}$ , known to exist in this compound under particular conditions of light exposure (wavelength and polarization direction) and temperature. The structure obtained for  $\text{MS}_\text{I}$  showed small but significant alterations in the Fe–N, Fe–C and N–O bonds along the *trans*-O–N–Fe–CN axis, relative to the ground state, also measured. Such changes are also possibly reflected in the anisotropic displacement parameters of the O and N atoms (see Table 2b in Rüdlinger *et al.*, 1992). The structure of  $\text{MS}_\text{II}$  indicated more marginal perturbations of the lengths of Fe–N and N–O bonds within the same molecular axis. Part of the incentive behind this structural work was the declared potential of SNP for application as an optical-storage device. Given that the ground state and two light-induced states of SNP display varied optical properties (Rüdlinger *et al.*, 1991), the structural characterization of each state was pertinent from a material-centred perspective as well as being innovative in an academic sense. This structural work led Coppens and co-workers to initiate X-ray diffraction experiments on SNP (Carducci *et al.*, 1997); their results revealed that the  $\text{MS}_\text{I}$  state undergoes a light-induced structural perturbation along the *trans*-NC–Fe–N–O axis, although their final interpretation of the data indicates ligand photoisomerization  $\text{Fe–NO} \rightarrow \text{Fe–ON}$  rather than a simple variation of bond length. Their structural characterization of  $\text{MS}_\text{II}$  yielded a further photoisomerization corresponding to the formation of a disordered  $\eta^2$ -bound NO moiety ligated to the Fe ion (Coppens *et al.*, 1998).

Coppens and co-workers then went on to demonstrate another type of photoisomerism:  $\eta^1$ - to  $\eta^2$ - $\text{SO}_2$  ligand isomerization in  $[\text{Ru}(\text{SO}_2)(\text{NH}_3)_4\text{Cl}]\text{Cl}$  and  $[\text{Ru}(\text{SO}_2)(\text{NH}_3)_4(\text{H}_2\text{O})](\text{tosylate})_2$  upon application of light at 355 nm, with each crystal sample held at 100 K to keep the  $\eta^2$ - $\text{SO}_2$  bound-state metastable (Kovalevsky *et al.*, 2002, 2003).

In the UK, Cole and co-workers used one of these photoisomers,  $[\text{Ru}(\text{SO}_2)(\text{NH}_3)_4(\text{H}_2\text{O})] \cdot [\text{tosylate}]_2$ , as a test material in the development of photo-induced X-ray crystallographic techniques at the synchrotron-radiation source (SRS) at Daresbury, UK. During these tests, the results of Coppens *et al.* were first reproduced and then several key experimental

parameters were varied in order to observe and to understand better their effect on the resultant refinement of the light-activated crystal structure (Bowes *et al.*, 2008). Temperature was one such parameter and, in one of these tests, a full data set was collected at 13 K. The results revealed a new type of photo-isomer that involves an end-on  $\eta^1$ -O bound Ru–OSO coordination (Bowes *et al.*, 2006). This example is the first of this type in ruthenium-based organometallic coordination chemistry whose structure has been published, as determined *via* the Cambridge Structural Database (Bruno *et al.*, 2002). At temperatures above those where Coppens and co-workers were investigating (100 K), the photo-isomerization remains metastable to about 240 K, above which its lifetime deteriorates progressively, attaining a lifetime of the order of microseconds near 295 K. Further data collections on this compound in a series were undertaken in the temperature range 250–280 K to investigate the associated progressive decrease in population of light-activated molecules as a function of temperature, which was revealed to be nearly linear.

More recently, Coppens and co-workers have demonstrated the first example of a single-crystal to single-crystal ‘double’ photoisomerization in  $[\text{Ru}(\text{bipyridine})_2(\text{NO})(\text{NO}_2)]\text{PF}_6$ , whereby the nitrosyl and nitro groups photoisomerize to isonitrosyl and nitrito ligands, respectively (Kovalevsky *et al.*, 2005). Here, photocrystallographic and supporting infrared spectroscopy results indicate that this isomerism occurs *via* intramolecular redox chemistry, involving oxygen transfer from the nitro to the nitrosyl group. Evidence has also been found for this type of linkage isomerism in an iron complex, (tetraphenylporphyrinato dianion) $\text{Fe}(\text{NO})(\text{NO}_2)$  *via* infrared measurements and density functional theory calculations (Novozhilova *et al.*, 2006).

Evidence for other types of metastable ligand photoisomer processes have been identified in the literature. In particular, complexes containing  $\eta^2$ - $\text{N}_2$ -, NO- and  $\text{SO}_2$ -based ligands have been described in the comprehensive review of ligand photoisomerization by Coppens *et al.* (2002). Clearly, therefore, there remains much scope for further work in this area.

The useful exploitation of host–guest chemistry in photo-crystallographic research has also been demonstrated by Coppens and co-workers. They have specifically synthesized host–guest complexes in which the guest is a photoactive species. Since the guest lies within a much larger host, one effectively ‘dilutes’ the photoactive species in a crystal this way so that the crystal lattice is stabilized even in the case of large structural changes (Coppens *et al.*, 2002). Therefore, one can augment the maximum fraction of excitation possible above which crystal fracture occurs (see §3). Various studies have been carried out, including the nice recent example of an *E*-to-*Z* photoisomerization in 2,3-dimethylacrylic acid when encased within a calixarene molecular framework (Zheng *et al.*, 2007).

The evident feasibility for determinations of light-induced metastable structures, hitherto described, has led to a further emerging field in photo-structural chemistry: that concerning the characterization of spin-crossing transitions in magnetic

materials. Spiering and co-workers reported the first direct observation of the well known light-induced excited-spin-state-transition (LIESST) effect by photo-induced single-crystal X-ray diffraction (Kusz *et al.*, 2001); the subject of this work was the complex  $[\text{Fe}(\text{mtz})_6](\text{BF}_4)_2$  (mtz = methyltetrazole), which undergoes a photo-induced transition from low spin to high spin (LS  $\rightarrow$  HS) at low temperature, and which is sufficiently stable at 10 K for data to be collected to determine the crystal structure corresponding to both the HS state, after irradiation ( $\lambda = 514 \text{ nm}$ ), and the LS state, obtained before photo-irradiation. The LIESST effect is evident *via* an extension of the Fe–N bond by  $\sim 0.2 \text{ \AA}$  which corresponds to the electronic transition  $^1A_1$  (LS)  $\rightarrow$   $^5T_2$  (HS). Complementary measurements of Mössbauer spectra indicate that complete photo-conversion occurs. Other steady-state single-crystal X-ray diffraction experiments have subsequently realized crystal structures of similarly photo-trapped Fe-containing complexes in a high-spin state, notably  $\text{Fe}(\text{phen})_2(\text{NCS})_2$  (phen = 1,10-phenanthroline) (Marchivie *et al.*, 2002), and Fe-based (pyrazol-1-yl)pyridine derivatives (Elhaik *et al.*, 2003, and references therein; Thompson *et al.*, 2005; Carbonera *et al.*, 2006). In these cases, changes of  $\sim 0.2 \text{ \AA}$  in Fe–N bond lengths again afford evidence of the spin transition. The photo-induced high-spin-state crystal structure in a bimetallic iron–silver complex,  $[\text{Fe}(\text{pyrimidine})][\text{Ag}(\text{CN})_2][\text{Ag}_2(\text{CN})_3]$ , has also been found (Niel *et al.*, 2005). In this case, the spin transition alters Ag $\cdots$ Ag distances as well as Fe–N bond distances.

Even more direct evidence for LIESST has been afforded in the pioneering work by Gillon and co-workers in which single-crystal polarized neutron diffraction has been exploited to observe the LIESST effect *via* the spatial distribution of the magnetization density in  $[\text{Fe}(\text{ptz})_6](\text{BF}_4)_2$  (ptz = 1-propyl-tetrazole), (Goujon *et al.*, 2003, 2006). The topological description of the magnetization density around the Fe-atom position corresponds well to that which one would expect from an  $\text{Fe}^{2+}$  magnetic form factor. Moreover, the magnetic moment on the Fe site was refined [to  $3.75$  (10)  $\mu_B$ ] and compared well with magnetic measurements [ $3.85 \mu_B$  (Goujon *et al.*, 2003)] and the theoretical value of the  $\text{Fe}^{2+}$  moment at saturation ( $3.84 \mu_B$ ). Such analysis yields a direct and quantitative measure of the fraction of photo-conversion, which, in

this case, was practically complete. The power of this technique is great as it stands to reveal unprecedented information about photo-induced magnetic effects that is key to the understanding of their physical properties. The great potential of bistable materials for memory devices and the great effort at present being exerted in industry to find materials for such applications reinforce the importance of this work.

## 6. The study of transient photo-excited phenomena

### 6.1. Luminescence: the origin of ‘molecular light’

Luminescence typically takes the form of either phosphorescence [type (iii) materials] or fluorescence [type (iv) materials] and it occurs when the ‘excited-state’ electrons relax back towards or into their original electronic energy state. This electronic relaxation is very fast, typically of the order of  $\mu\text{s}$  or ns and very frequent, and so, whilst the observed luminescence typically appears to be static, it actually represents a continuous stream of many  $\mu\text{s}$ -to- $\text{ps}$ -lived pulses of light.

Phosphorescence is associated with the slower end of this range of lifetimes (typically  $\mu\text{s}$ ) whilst ns lifetimes are classically characteristic of fluorescence. The reason for this difference in lifetime is that excited electrons may relax *via* a transition from triplet-to-singlet or singlet-to-singlet energy levels, the former being quantum-mechanically forbidden such that relaxation is slowed down by an intersystem crossing pathway (phosphorescence), whilst the latter is a direct transition between two quantum-mechanically allowed energy levels (fluorescence). These processes are illustrated in Fig. 3. An overview of the time scales of photochemical reactions in solids has been given by Davaasambu *et al.* (2004).

Luminescent molecules are key building blocks in materials for molecular wires, light-emitting diodes (LEDs) and new optical display-screen technology. Getting the right energy match between the incident light and the absorption energy between the ground-state energy level and the first-excited-state energy level (the so-called ‘band gap’) is fundamental to ensuring good brightness levels of luminescence and long-term light production in ultimate device operation.

### 6.2. The need for the development of time-resolved ‘photo-crystallography’

In order to best exploit the luminescent attributes of target organic and organometallic compounds for device operation, one needs to harness the structural form of these excited-state luminescent species. Whilst optical spectroscopy is able to provide indirect information about the likely dominant character of the excited state, only crystallography can offer a route to the full three-dimensional geometry of this excited-state structure. Knowledge of this structure, in comparison to the ground-state structure, would illustrate directly the nature of the redistribution of electrons in the excited state.

Since the excited states of luminescent materials are so ephemeral (typically  $\mu\text{s}$ – $\text{ps}$ ), one needs to use existing small-molecule single-crystal diffraction methodologies in combination with stroboscopic (optical)pump-(X-ray)probe

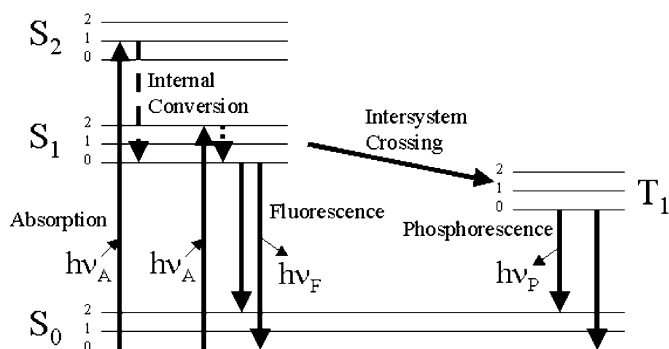


**Figure 3**  
Energy-level diagram illustrating fluorescence and phosphorescence.

technology. Here, a pulsed X-ray source is synchronized with a pulsed laser beam using phase-locking techniques, such that the sample is photo-excited repetitively at the same time as it is probed with X-ray diffraction. The time scale of this stroboscopic process must be set such that data are captured before the light-activated effect falls off, *i.e.* it must be significantly shorter than the specific ( $\mu\text{s}$ – $\text{ps}$ ) lifetime of the photo-induced excited state in the sample in order to observe the photo-structural perturbation. Fig. 4 illustrates these time-structure requirements.

One needs to use a pulsed X-ray source since a continuous source would allow the collection of diffraction data from the pure ground-state structure (seen between laser pulses) as well as the already heavily ground state dominated structural signature that lies on top of the small fraction of unit cells wherein the photo-excited state is observed. In other words, the desired photo-structural effect will be too heavily diluted by the ground state to observe it unless the time-averaged wholly ground state signature is removed by collecting diffraction data only during the repetitive times when the sample is photo-excited.

The required  $\mu\text{s}$ – $\text{ns}$  X-ray pulses can be obtained by use of either (i) a mechanical X-ray chopper or (ii) the inherent temporal structure of the particle accelerator of a synchrotron. In order to retain the highest duty cycle possible, *i.e.* the overall percentage of time that the sample is exposed to X-rays, we use a mechanical chopper where sample photolifetimes are at least a microsecond, and the temporal structure of a synchrotron to study more transient photostructural phenomena down to picoseconds.

Whilst such time-resolved X-ray photocrystallography experiments are so technically challenging, by embracing this much more complex *time-resolved* dimension, one can benefit enormously. For example, one can envisage, ultimately, being able to capture images or ‘molecular movies’ that represent the evolution of such short-lived species, and therefore visualize the step-by-step evolution of any optical or optoelectronic effect. In the wider context, one could apply this characterization tool to follow any photo-induced phenomenon or reaction pathway. Indeed, some very impressive

movies of reaction pathways have recently been constructed that describe ground-breaking work in macromolecular (biological) crystallography (*e.g.* see Perman *et al.*, 1998; Schotte *et al.*, 2003, 2004). It is worth adding that picosecond-resolution time-resolved photoreaction kinetics have also been followed in liquid diffraction studies (*e.g.* Ihee *et al.*, 2005; Davidsson *et al.*, 2005; Kim *et al.*, 2006; Wulff *et al.*, 2006), although this is slightly out of the scope of crystallography.

### 6.3. Technical aspects of time-resolved photocrystallography

**6.3.1. Pulsed X-rays via a mechanical chopper [for type (iii) materials].** For samples with photo-active lifetimes down to  $\mu\text{s}$ , a mechanical chopper can be used to afford X-ray pulses. Ozawa *et al.* (1998) gave an example of one such chopper design, in which a rotating chopper operates a wheel comprising slits of varying width radially. To access the greatest possible range of X-ray pulse lengths, this wheel is removable from the chopper such that one of several wheels, each with a separate range of slit apertures, can be chosen for a given experiment. An adaptation of this chopper with a greater speed and rate of repetition has more recently been developed (Gembicky *et al.*, 2005). This adaptation affords sub-microsecond time structure that can be used to isolate one X-ray pulse produced by a synchrotron that delivers picosecond X-ray pulses (Gembicky & Coppens, 2007). Such a design is now used at the Advanced Photon Source, Argonne National Laboratories, Chicago, USA.

An alternative chopper design that requires no removal of a wheel has been developed by Cole and co-workers (Husheer *et al.*, 2005; Husheer, 2007). This chopper has two blades comprising two circular discs, each of identical design. The two discs are aligned parallel to each other and positioned perpendicular to the incident continuous beam of X-rays such that the X-rays meet each chopper disc at its outer perimeter. Half the outer perimeter on the rim of each disc is etched away, thus permitting X-rays to pass freely through a half revolution of each disc. The two discs operate together to achieve a variable length of X-ray pulse: this variability is achieved on rotating both discs in the same sense to each other and at the same frequency (10–30 Hz is possible), but allowing the relative positions of the open (outer) part of each rim to be adjusted independently. For example, if the relative positions of each disc are almost identical, a large X-ray aperture (longer X-ray pulse) results (Fig. 5); conversely, if the relative positions of each disc are almost counter to each other, a small X-ray aperture per disc revolution (short X-ray pulse) is obtained (see Fig. 5). The relative positions of the two discs might also lie anywhere between these two extremes, which are  $180^\circ$  apart, thus yielding a continuous range of X-ray pulses *via* this design. Fully programmable data array and timing logic allow the relative positions of each disc to be adjusted independently and in a controllable way. The limits of X-ray pulses in this range are determined by the speed of revolution of the chopper and the circumference of each disc. The design of this particular chopper allows synchrotron-based time resolution from ms to  $\mu\text{s}$ .

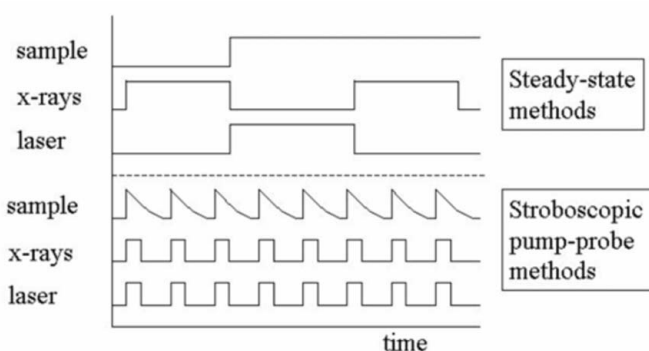


**Figure 4**

A schematic diagram of the relative timing systems between laser, X-ray and sample photo-conversion lifetime.

For each chopper design featured above, the rate of repetition of the X-ray pulses is matched with that of the pulsed laser and the timing of the opening of the chopper is synchronized to the shutter opening of the laser such that both the optical and X-ray pulses are either ‘on’ or ‘off’ at a given instant. The ‘on’ periods thereby correspond to the structure of the  $x\%$  photo-converted state combined with that of the  $100 - x\%$  non-photo-absorbed ground state, whereas the ‘off’ periods relate to the fully recovered ground state. Each frame of data thus acquires Bragg intensity exclusively from the ‘on’ periods; during the ‘off’ periods, only background is accrued. The preclusion of any contamination of Bragg intensity due to the exclusive ground-state structure avoids heavy dilution of the contrast that is sought between the ground and light-induced structures: such contamination would present an insurmountable problem. Dark time in a significant amount is introduced in this experimental method. Consequently, although a laboratory X-ray source might be used for many steady-state experiments (even though the greater flux of synchrotron radiation would invariably increase the contrast), synchrotron radiation is mandatory for experiments of these types in which X-ray pulses are created – the much greater X-ray flux available at a synchrotron is required to compensate for the highly depleted time-averaged flux (low ‘duty cycle’) caused on pulsing the X-rays.

In terms of strategies to collect data, interleaving the data frames for the exclusive ground state and ‘ground + light-induced’ data sets is important when employing this method. ‘Interleaving’ involves each ‘light-on’ and ‘light-off’ data frame being collected one immediately after the other for each angular setting. This not only optimizes the angular coverage of reciprocal space per unit time, as there is less motor drive,

but it is much more time efficient since the stroboscopic process inherently provides for an alternate ‘light-on’ and ‘light-off’ data collection. In order to facilitate this ‘interleaving’ data-collection process, a mechanism of electronic timing is established between the laser shutter and the software to control the diffractometer such that this process can be repeated automatically.

Data-interleaving strategies are also highly advantageous to minimize the danger of sample decay. If the crystal were to fracture halfway through an experiment in which this alternating ‘light–dark’ strategy was in use, at least half the data collected could be analysed. Conversely, there is little use in analysing a full ground-state data collection together with data collection from the light-induced crystal for ten minutes, at which point the crystal fractured, as insufficient data would be available to perform a ‘light–dark’ comparative analysis of data. This alternating strategy also allows for the effects of gradual sample decay to be corrected much more easily than if the data had been collected on the ground state exclusively first, because the level of any decay is about the same where each ‘data frame pair’ is collected one after the other. Other time-dependent systematic effects can likewise be eradicated, particularly the effects of synchrotron-beam decay if X-rays from this source are used for the experiment. One additional feature of the design of such an experiment that removes systematic effects is the collection of ground and ‘ground + light-induced’ data on the same detector-image frame by shifting the detector by a small and known amount between the collection of data from each of the two states. Systematic errors such as varying ratios of signal to noise between frames are thereby avoided. Such an approach has been demonstrated successfully using image-plate detectors (Ozawa *et al.*, 2003) but such a method is suitable only where diffracted spots present on the image are not so many that a detector shift is impossible without reflections from one of these images overlapping with some of those from the second image.

As the duty cycle is small when pulsed X-rays are used, one must collect a frame of data for a considerable duration to afford Bragg signals of adequate intensity. This condition contrasts with a steady-state experiment in which one has generally the luxury of collecting data with satisfactory statistics because, here, the detector read-out time, rather than the rate of data collection, is the time-limiting factor of an experiment. Consequently, owing to practical time constraints, one must generally compromise the accuracy of the Bragg intensities over a realistic time frame to perform an experiment that utilizes X-ray pulses. Such a compromise most affects the viability of observing the results sought where the fraction of photo-conversion is small. In these cases, it is considered better to analyse the *difference* between two intensities collected in rapid succession, as this condition yields results more accurate than the parent intensities themselves due to the avoidance of various systematic effects. This effect has been found in similar crystallographic difference experiments in which the differences sought are similarly small (Paturle *et al.*, 1991). In such cases, the reflection intensities are derived from the response ratio,  $\eta$ , according to

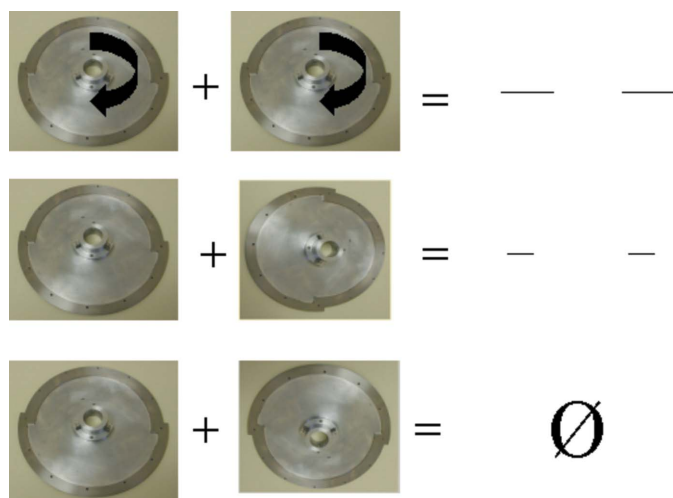


**Figure 5**

Two discs of the mechanical chopper developed by Cole and co-workers (Husheer *et al.*, 2005). When operational, the discs lie parallel to each other and the X-rays are fired at the outer rim of each disc, perpendicular to the disc surface. The X-ray pulse lengths are determined from the relative positioning of wheels with respect to each other, *e.g.* in phase (top), one rotated  $90^\circ$  to the other (middle), and completely out of phase to each other (bottom).

$$\eta_{hkl} = \frac{I_{\text{on}}(hkl) - I_{\text{off}}(hkl)}{I_{\text{off}}(hkl)} = \frac{I_{\text{on}}(hkl)}{I_{\text{off}}(hkl)} - 1, \quad (1)$$

in which  $I_{\text{on}}$  is the intensity of the light-activated state and  $I_{\text{off}}$  represents the conventional ground-state Bragg intensity. The response ratios can be refined by least-squares methods using derivative expressions of  $\eta$  (Ozawa *et al.*, 1998). More recent work illustrates the importance of statistical Wilson plots in determining a least-squares-refinement starting value for the temperature factor of each atom in the photo-induced species (Vorontsov & Coppens, 2005). The importance of theoretical predictions of Bragg intensity changes upon photo-excitation, calculated from first principles, has also been proven (Debnarova *et al.*, 2006). Similarly, kinetic theory for various time laws can be applied in cases where thermal equilibrium of the microenvironment is assured (Techert, 2004).

**6.3.2. Pulsed X-rays via the temporal structure of a synchrotron [for type (iv) materials].** For samples with photo-active lifetimes from  $\mu\text{s}$  to ps, the temporal structure of a synchrotron is exploited to realize matching  $\mu\text{s}$ –ps X-ray pulses. This temporal structure derives from the fact that the electrons that are accelerated around a synchrotron ring, before being agitated magnetically to emit X-rays, circulate in discreet bunches. The ‘bunch width’ is described in terms of the duration that the full length of an electron bunch takes to pass a given point in the synchrotron, a time scale of order ns to ps. Accelerator physics can be used to harness these bunches individually to provide pulsed X-rays on a ns–ps timescale, or they can be grouped together with other bunches to create a train of X-ray pulses of, in principle, any time scale up to the limiting orbit speed of the synchrotron (of order  $\mu\text{s}$ ) that would correspond to the head of this train of pulses joining its own tail in the synchrotron circuit. Thus, X-ray pulses on a time scale from  $\mu\text{s}$  to ps are available. In practice, there are restrictions on the exact time scales available as a synchrotron operates in one of a small selection of ‘bunch

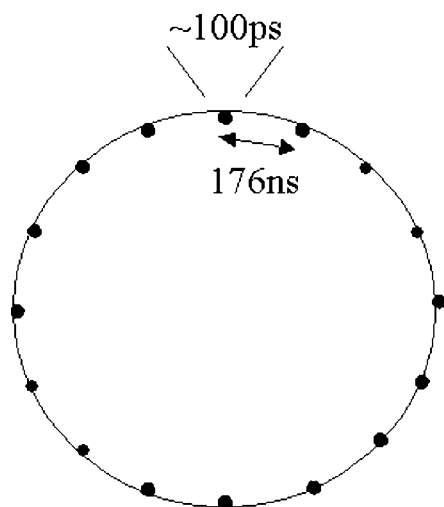


**Figure 6**  
One of the (16-bunch) time structures available in the synchrotron at the ESRF, Grenoble, France.

modes’ because the X-ray source serves simultaneously many instruments, some of which require no such time structure but, in contrast, require as great an X-ray intensity (thus high duty cycle) as possible. Certain bunch modes are thereby available in a synchrotron at various times during the year. As an illustration, Fig. 6 shows the 16-bunch mode that is available at the ESRF, Grenoble, France. One can fine tune the time frame of the X-ray pulse desired for a given experiment by combining this inherent timing with a chopper that isolates one of these bunches from the 16 available. One such chopper, used on the ID9 beamline at the ESRF, is described by Bourgeois *et al.* (1996).

To utilize the pump-probe method for such experiments, one can use a laser of ns, ps or fs pulse width, any of which is commercially available, with high-speed electronics such that the required time-gated synchronization between X-ray and laser pulses for the experiment is achieved.

The much shorter X-ray pulses, used in these experiments, result in such a low duty cycle that obtaining sufficient X-ray flux is challenging at even the most powerful synchrotrons. Only in 1998 were the first results achieving nanosecond temporal resolution published, nearly two decades after the first feasibility studies of the technique. The first attempt at time gating a synchrotron X-ray pulse to a laser pulse was conducted in 1980–1 with an extended X-ray absorption fine-structure (EXAFS) experiment (Sandstrom *et al.*, 1980, 1981), but all attempts failed primarily due to instabilities of the beam accelerator. A reinvestigation of this method in 1984 achieved success on the millisecond time scale, again employing EXAFS techniques (Mills *et al.*, 1984). Significant improvements in synchrotron technology made during these two decades were required to enable these ideas to be rejuvenated with success and applied to diffraction; even now there are only a few publications of such results arising from ns–ps temporally resolved crystallography of photo-active species. Of these studies, most have comprised the characterization of transient biological species on the ns time scale and have utilized Laue diffraction techniques (*cf.* Bragg’s law: varying  $\lambda$ , fixed  $\theta$ ) rather than monochromatic oscillatory based methods (*cf.* Bragg’s law: varying  $\theta$ , fixed  $\lambda$ ), which are the principal subject of this review. Laue diffraction has the great advantage of rapid acquisition of data, as the Bragg condition is met many times simultaneously when  $\lambda$  is the variable parameter.

Although oscillatory methods afford data much more slowly than Laue diffraction, they have the intrinsic advantage over Laue diffraction that they preclude the overlap of reflections, as one can assume that the Bragg condition is met only once at a given time in experiments with diffraction of monochromatic X-rays. There is thus no need to deconvolve reflections that commonly hamper the resolution of the data in Laue diffraction, in which reflection overlap is prevalent because the Bragg condition is met many times simultaneously. As the light-induced chemical changes in these experiments are generally on a molecular scale and are typically subtle, great atomic resolution is a prerequisite, thus making Laue diffraction problematic. In the aforementioned

biological studies, distinct areas of electron density which appear in Fourier-difference maps upon creation of the transient species were revealed rather than individual perturbations on an atomic scale. In addition, instrumentally, Laue diffraction requires X-rays in a white beam that comprises X-ray wavelengths in a continuous range acting simultaneously on the sample. All Laue-based experiments are therefore restricted instrumentally to synchrotron sources.

This all said, Laue diffraction is at present the only viable method to use in experiments in which the crystals deteriorate quickly upon photo-activation. Moreover, large strides in the development of Laue-based X-ray crystallography have been made recently both in software (Ren *et al.*, 1999) and hardware, and one can look forward to an exciting future in this regard in small-molecule crystallography as well as macromolecular crystallography. In particular, recently developed 'multilayer' wavelength-band selection that is available at the latest generation synchrotron sources enables an intense and focused 'pink-beam' option (Hignette *et al.*, 2005; Englich *et al.*, 2005; Stoermer *et al.*, 2007). This is a pseudo-Laue configuration in the sense that it permits a few percent of the full white-beam bandwidth through to the sample. This fine-wavelength-band selection largely avoids the peak overlap problem associated with white-beam experiments, whilst providing more rapid acquisition of data than conventional oscillatory monochromatic methods would allow. One should note that the use of pink or white synchrotron beams affords a substantial heat load on downstream beamline instrument components in time-resolved photocystallography experiments. This is because the stroboscopic pump-probe process of such experiments is sustained over a long period of time, thus causing heat to build up. Water-cooled heat-load shutters have recently been installed on a number of beamlines in order to successfully combat this problem (Gembicky *et al.*, 2007).

#### 6.4. Time-resolved photo-crystallography results to date

In the microsecond time-resolved (non-steady-state) regime, thus far there exist results on only a few complexes. The first recorded result concerns the anion  $\text{Pt}_2(\text{pop})_4^{4-}$  (pop = pyrophosphate,  $[\text{H}_2\text{P}_2\text{O}_5]^{2-}$ ). The groups of Coppens and Ohashi have independently deduced significant light-induced contraction of the Pt–Pt bond [ $\Delta = -0.23$ – $-0.28$  (9) Å] in this ion according to single-crystal X-ray diffraction. Separate counterions were used: Coppens used  $[\text{N}(\text{C}_2\text{H}_5)_4](\text{H})$  whereas Ohashi used  $[\text{N}(\text{C}_5\text{H}_{11})_4]_2(\text{H})_2$ . Although the results are similar, one would thus expect minor variation due to the slightly varied molecular environments surrounding the anion in the crystal lattice. The two groups also used separate experimental techniques: Coppens utilized stroboscopic pump-probe methods that exploit the aforementioned mechanical-chopper design on the X3 beamline at the NSLS, Brookhaven, USA, with 50  $\mu\text{s}$  resolution and at liquid-helium temperature (Kim *et al.*, 2002); Ohashi and co-workers used pseudo-steady-state methods, both in the laboratory (Yasuda *et al.*, 2002) and on the BL02B1 beamline at the SPring-8 synchrotron, Japan (Ozawa *et al.*, 2003). The extent of Pt–Pt

bond contraction in each case is identical within experimental error, and is consistent also with results from EXAFS, electronic and optical spectral measurements (Fordyce *et al.*, 1981; Stein *et al.*, 1983; Thiel *et al.*, 1993a,b) despite the use of distinct counterions. The results are all compatible with a rationalization that the promotion of a Pt–Pt antibonding  $d\sigma^*$  electron into a weakly bonding  $p$  orbital is responsible for this structural change. The work by Coppens and co-workers shows that a concurrent rotation by  $3^\circ$  of the Pt–Pt axis in the plane that bisects two Pt–P vectors occurs in this photo-excitation. Subsequent complementary density functional theory (DFT) calculations have been performed (Novozhilova *et al.*, 2003); their results are consistent with the experimental results, except that they show some discrepancy with the EXAFS results in terms of the associated Pt–P bond changes. This effect is unsurprising given the expected propensity of multiple scattering in the EXAFS spectra that might occlude the true Pt–P distance, and the challenging nature of DFT calculations to deduce  $M$ – $M$  bond distances in directly bound third-row transition-metal excited states.

Given the highly developmental nature of such pump-probe diffraction experiments coupled with the subtlety of the structural variations sought, obtaining consistency with analogous spectral and theoretical results is important for a quantitative assessment of the reliability of the results and thus the progress of this field. In this regard, Coppens and co-workers performed DFT calculations on a bis(2,9-dimethyl-1,10-phenanthroline)copper(I) ion (Chen *et al.*, 2003), of which the metal–ligand charge-transfer (MLCT) excited state had been characterized by Chen and co-workers (Chen *et al.*, 2002) using stroboscopic pump-probe EXAFS measurements at the Advanced Photon Source, Argonne, USA, which employs the temporal structure of the synchrotron. A mechanical-chopper-based temporally resolved pump-probe X-ray diffraction experiment was subsequently performed by Coppens and co-workers on a similar Cu complex, the sole difference being the substitution of one phenanthroline ligand for a 1,2-bis(diphenylphosphino)ethane ligand (Coppens, Vorontsov *et al.*, 2004). In the X-ray diffraction experiment, the lowest triplet excited state with a lifetime of 85  $\mu\text{s}$  at 16 K was probed. The structure was refined using response ratios, as described earlier in §6.3.1, and marked displacements of the Cu atom in each of two independent molecules in the unit cell were observed. In a similar experiment, a significant contraction ( $\sim 0.85$  Å) of an Rh–Rh bond was observed in the ion  $[\text{Rh}_2(1,8\text{-diisocyno-}p\text{-menthane})_4]^{2+}$  in its excited triplet state that possesses a lifetime of 11.7  $\mu\text{s}$  at 23 K (Coppens, Gerits *et al.*, 2004). A year later, Coppens *et al.* reported the first photocystallographic structure determination of a transient intermolecular excimer (Vorontsov *et al.*, 2005). The experiment investigated the nature of the 53 (1)  $\mu\text{s}$  phosphorescent state of  $\{[3,5\text{-}(\text{CF}_3)_2\text{pyrazolate}]\text{Cu}\}_3$  at 17 K upon exposure to 355 nm. In the ground state, the molecules stack in a columnar configuration, with alternating intermolecular Cu...Cu separations of 3.787 (1) and 4.018 (1) Å. Results showed that, in the phosphorescent state, the longer of these two separations contracted from 4.018 (1) to 3.46 (1) Å whilst

the shorter separation increased from 3.610 (1) to 3.91 (1) Å. Photo-irradiation therefore causes a dimerization effect, rather than a simple compression as one might intuitively expect.

In parallel to this work, several small-molecule single-crystal diffraction experiments have been conducted in Europe, using the ID9 beamline at the European Synchrotron Radiation Facility (ESRF), Grenoble, France. The most celebrated of such studies is the photo-induced paraelectric (neutral) to ferroelectric (ionic) structural phase transition in tetrathiafulvalene-*p*-chloranil [TTF-CA] (Collet *et al.*, 2003). Here, a 300 fs pulsed-laser pump and a 100 ps X-ray probe were used to deduce the structure of its ground state and photo-induced state, data being collected stroboscopically 2 ns before and 1 ns after each laser pulse. Before data collection, the phase transition proceeds *via* cooperative accumulation of each photo-induced molecule such that there is a lead time of ~500 ps required for the effect to convert from a molecular to a macroscopic phenomenon. Accordingly, the evolution of the photo-induced state was monitored before the data collection on recording the changes in relative intensity of certain Bragg reflections over the time scale 0–500 ps. Other experiments have involved similar experimental arrangements to investigate transient structures with lifetimes from ps to ns. For instance, Cole and co-workers used ID9 at the ESRF to probe the ephemeral <sup>3</sup>MLCT state of a rhenium carbene complex, [HNCH<sub>2</sub>CH<sub>2</sub>NHCr(2,2'-bipyridine)(CO)<sub>3</sub>]Br, which has a lifetime of ~230 ns (Cole *et al.*, 2003); the feasibility of the experiment was confirmed in terms of the experimental arrangement and structural simulations. Accordingly, data were collected and initial indications from data analysis show that the experiment has been successful. Although this review focuses on single-crystal X-ray diffraction, we also mention the powder X-ray diffraction study as it was the first to report ps-time-resolved photo-induced structural changes in a small molecule; it concerned the organic compound (*N,N*-dimethylamino)benzonitrile [DMABN] (Tchert *et al.*, 2001).

## 7. Concluding remarks and outlook

We have detailed the current state of the field of photocrystallography using small-molecule X-ray diffraction. The techniques available to us presently allow the three-dimensional structural characterization of reversible and irreversible solid-state photo-structural changes, and the structural manifestations associated with the formation of molecular excited states. The structures of both long-lived and transient light-induced molecular species can be captured, down to a pico-second photo-induced lifetime using current technology.

For the future, we are likely to see more use of the μs–ps time-resolved regime, including the application of pink-beam and Laue experimentation, given the good prospects of new-generation synchrotron sources. In addition, there is already large investment in new technologies that will enable even faster time scales to be accessed, of the order of femtoseconds. Such technologies are based on laser-sliced synchrotron emission (Schoenlein *et al.*, 2000), high harmonic generation

(Spielmann *et al.*, 1997; Chang *et al.*, 1997), linear-accelerator-based X-ray free-electron lasers (Service, 2002; Blome *et al.*, 2005) with enhanced timing synchronization using electro-optic sampling (Cavalieri *et al.*, 2005), and laser-induced plasma physics (Rischel *et al.*, 1997; Tompkins *et al.*, 1998). This time frame corresponds to that commonly associated with the bond-breaking and bond-making phenomena. Therefore, photocrystallographic experiments on this time scale should ultimately allow us to observe the structural dynamics of solid-state photochemical reactions in the form of a molecular movie.

Increasingly, corroborative evidence is also likely to feature in reports concerning photocrystallography experiments, by way of spectroscopy of theoretical calculations. This draws on the continuing advances in density functional theory and general progress in theory that is starting to catch up with this novel experimental area. The more routine nature and desktop design of modern infrared and optical spectroscopic instrumentation is also a factor in this trend.

In terms of industrial application, the results of the work will enable the establishment of excited-state structure–photophysical property relationships, otherwise unobtainable at present in any direct three-dimensional or quantitative manner, and this knowledge will be used subsequently to optimize these properties. This leads to the ultimate goal of being able to tailor the structure of a material to meet the desired physical property specifications of a given photonic application.

The author wishes to thank the Royal Society for a University Research Fellowship and St Catharine's College, Cambridge, for a Senior Research Fellowship.

## References

- Blome, C., Tschentscher, Th., Davaasambuu, J., Durand, P. & Techert, S. (2005). *J. Synchrotron Rad.* **12**, 812–819.
- Bourgeois, D., Ursby, T., Wulff, M., Pradervand, C., Legrand, A., Schildkamp, W., Labouré, S., Srajer, V., Teng, T. Y., Roth, M. & Moffat, K. (1996). *J. Synchrotron Rad.* **3**, 65–74.
- Bowes, K. F., Cole, J. M., Husheer, S. L. G., Raithby, P. R., Savarese, T. L., Sparkes, H. A., Teat, S. J. & Warren, J. E. (2006). *Chem. Commun.* pp. 2448–2450.
- Bowes, K. F., Cole, J. M., Husheer, S. L. G., Raithby, P. R., Sparkes, H. A., Teat, S. J. & Warren, J. E. (2008). *J. Synchrotron Rad.* In the press.
- Brinkman, W. F. & Pinto, M. R. (1997). *Bell Labs Tech. J.* pp. 57–75.
- Bruno, I. J., Cole, J. C., Edgington, P. R., Kessler, M., Macrae, C. F., McCabe, P., Pearson, J. & Taylor, R. (2002). *Acta Cryst.* **B58**, 389–397.
- Carbonera, C., Sanchez Costa, J., Money, V. A., Elhaik, J., Howard, J. A. K., Halcrow, M. A. & Letard, J.-F. (2006). *J. Chem. Soc. Dalton Trans.* **25**, 3058–3066.
- Carducci, M. D., Pressprich, M. R. & Coppens, P. (1997). *J. Am. Chem. Soc.* **119**, 2669–2678.
- Cavalieri, A. L., Fritz, D. M., Lee, S. H., Bucksbaum, P. H., Reis, D. A., Rudati, J., Mills, D. M., Fuoss, P. H., Stephenson, G. B., Kao, C. C., Siddons, D. P., Lowney, D. P., MacPhee, A. G., Weinstein, D., Falcone, R. W. *et al.* (2005). *Phys. Rev. Lett.* **94**, 114801.
- Chang, Z. H., Rundquist, A., Wang, H. W., Murnane, M. M. & Kapteyn, H. C. (1997). *Phys. Rev. Lett.* **79**, 2967–2970.

- Chen, L. X., Jennings, G., Liu, T., Gosztola, D. J., Hessler, J. P., Schalltrito, D. V. & Mayer, G. J. (2002). *J. Am. Chem. Soc.* **124**, 10861–10867.
- Chen, L. X., Shaw, G. B., Novozhilova, I., Liu, T., Jennings, G., Attenkofer, K., Mayer, G. J. & Coppens, P. (2003). *J. Am. Chem. Soc.* **125**, 7022–7034.
- Cohen, M. D. & Schmidt, G. M. J. (1964). *J. Chem. Soc.* pp. 1996–2000.
- Cole, J. M. (2004). *Chem. Soc. Rev.* **33**, 501–513.
- Cole, J. M., Raithby, P. R., Wulff, M., Schotte, F., Plech, A., Teat, S. J. & Bushnell-Wye, G. (2003). *Faraday Discuss.* **122**, 119–129.
- Collet, E., Lemee-Cailleau, M.-H., Buron-Le Cointe, M., Cailleau, H., Wulff, M., Luty, T., Koshihara, S.-Y., Meyer, M., Toupet, L., Rabiller, P. & Techert, S. (2003). *Science*, **300**, 612–615.
- Coppens, P., Formitchev, D. V., Carducci, M. D. & Culp, K. (1998). *Dalton Trans.* **6**, 865–872.
- Coppens, P., Gerlits, O., Vorontsov, I. I., Kovalevsky, A. Y., Chen, Y.-S., Graber, T., Gembicky, M. & Novozhilova, I. V. (2004). *Chem. Commun.* **19**, 2144–2145.
- Coppens, P., Ma, B., Gerlits, O., Zhang, Y. & Kulshrestha, P. (2002). *CrystEngComm*, **4**, 302–309.
- Coppens, P., Novozhilova, I. & Kovalevsky, A. (2002). *Chem. Rev.* **102**, 861–883.
- Coppens, P., Vorontsov, I. I., Graber, T., Kovalevsky, A. Y., Chen, Y.-S., Wu, G., Gembicky, M. & Novozhilova, I. V. (2004). *J. Am. Chem. Soc.* **126**, 5980–5981.
- Davaasambuu, J., Busse, G. & Techert, S. (2006). *J. Phys. Chem. A*, **110**, 3261–3265.
- Davaasambuu, J., Durand, P. & Techert, S. (2004). *J. Synchrotron Rad.* **11**, 483–489.
- Davidsson, J., Poulsen, J., Cammarata, M., Georgiou, P., Wouts, R., Katona, G., Jacobson, F., Plech, A., Wulff, M., Nyman, G. & Neutze, R. (2005). *Phys. Rev. Lett.* **94**, 245503.
- Debnarova, A., Techert, S. & Schmatz, S. (2006). *J. Chem. Phys.* **125**, 224101.
- Elhaik, J., Money, V. A., Barrett, S. A., Kilner, C. A., Radosavljevic Evans, I. & Halcrow, M. A. (2003). *J. Chem. Soc. Dalton Trans.* **10**, 2053–2060.
- Englich, U., Kazimirov, A., Shen, Q., Bilderback, D. H., Gruner, S. M. & Hao, Q. (2005). *J. Synchrotron Rad.* **12**, 345–348.
- Fordyce, W. A., Brummer, J. G. & Crosby, G. A. (1981). *J. Am. Chem. Soc.* **103**, 7061–7064.
- Furusawa, T., Kawano, M. & Fujita, M. (2007). *Angew. Chem. Int. Ed.* **46**, 5717–5719.
- Gembicky, M., Adachi, S. & Coppens, P. (2007). *J. Synchrotron Rad.* **14**, 295–296.
- Gembicky, M. & Coppens, P. (2007). *J. Synchrotron Rad.* **14**, 133–137.
- Gembicky, M., Oss, D., Fuchs, R. & Coppens, P. (2005). *J. Synchrotron Rad.* **12**, 665–669.
- Goujon, A., Gillon, B., Debede, A., Cousson, A., Gukasov, A., Jetic, J., McIntyre, G. J. & Varret, F. (2006). *Phys. Rev. B*, **73**, 104413.
- Goujon, A., Gillon, B., Gukasov, A., Jetic, J., Nau, Q., Codjovi, E. & Varret, F. (2003). *Phys. Rev. B*, **67**, 220401.
- Hashizume, D. & Ohashi, Y. (1999). *J. Chem. Soc. Perkin Trans. 2*, **8**, 1689–1694.
- Hignette, O., Cloetens, P., Rostaing, G., Bernard, P. & Moreawe, C. (2005). *Rev. Sci. Instrum.* **76**, 063709.
- Husheer, S. L. G. (2007). PhD thesis, University of Cambridge, UK.
- Husheer, S. L. G., Cole, J. M., Teat, S. J., Warren, J. E. & Bushnell-Wye, G. (2005). Proceedings of the British Crystallographic Association Spring Meeting, Loughbrough, UK, Abstract CP-28.
- Ihee, H., Lorenc, M., Kim, T. K., Kong, Q. Y., Cammarata, M., Lee, J. H., Bratos, S. & Wulff, M. (2005). *Science*, **309**, 1223–1227.
- Kawano, M., Hirai, K., Tomioka, H. & Ohashi, Y. (2007). *J. Am. Chem. Soc.* **129**, 2383–2391.
- Kawano, M., Ozawa, Y., Matsubara, K., Imabayashi, H., Mitsumi, M., Toriumi, K. & Ohashi, Y. (2002). *Chem. Lett.* pp. 1130–1131.
- Kim, T. K., Lorenc, M., Lee, J. H., Lo Russo, M., Kim, J., Cammarata, M., Kong, Q., Noel, S., Plech, A., Wulff, M. & Ihee, H. (2006). *Proc. Natl Acad. Sci.* **103**, 9410–9415.
- Kim, C. D., Pillet, S., Wu, G., Fullagar, W. K. & Coppens, P. (2002). *Acta Cryst. A* **58**, 133–137.
- Kovalevsky, A. Y., Bagley, K. A., Cole, J. M. & Coppens, P. (2003). *Inorg. Chem.* **42**, 140–147.
- Kovalevsky, A. Y., Bagley, K. A. & Coppens, P. (2002). *J. Am. Chem. Soc.* **124**, 9241–9248.
- Kovalevsky, A. Y., King, G., Bagley, K. A. & Coppens, P. (2005). *Chem. Eur. J.* **11**, 7254–7264.
- Kusz, J., Spiering, H. & Gütlich, P. (2001). *J. Appl. Cryst.* **34**, 229–238.
- McBride, J. M. (1983). *Acc. Chem. Res.* **16**, 304–312.
- Marchivie, M., Guionneau, P., Howard, J. A. K., Chastanet, G., Letard, J.-F., Goeta, A. E. & Chasseau, D. (2002). *J. Am. Chem. Soc.* **124**, 194–195.
- Mills, D. M., Lewis, A., Harootunian, A., Huang, J. & Smith, B. (1984). *Science*, **223**, 811–813.
- Nakanashi, H., Jones, W., Thomas, J. M., Hursthouse, M. B. & Motevalli, M. (1980). *J. Chem. Soc. Chem. Commun.* **13**, 611–612.
- Nakanashi, H., Jones, W., Thomas, J. M., Hursthouse, M. B. & Motevalli, M. (1981). *J. Phys. Chem.* **85**, 3636–3642.
- Niel, V., Thompson, A. L., Goeta, A. E., Enachescu, C., Hauser, A., Galet, A., Muñoz, M. C. & Real, J. A. (2005). *Chem. Eur. J.* **11**, 2047–2060.
- Novozhilova, I. V., Coppens, P., Lee, J., Richter-Addo, G. B. & Bagley, K. A. (2006). *J. Am. Chem. Soc.* **128**, 2093–2104.
- Novozhilova, I. V., Volkov, A. V. & Coppens, P. (2003). *J. Am. Chem. Soc.* **125**, 1079–1087.
- Ohhara, T., Harada, J., Ohashi, Y., Tanaka, I., Kumazawa, S. & Niimura, N. (2000). *Acta Cryst. B* **56**, 245–253.
- Ozawa, Y., Pressprich, M. R. & Coppens, P. (1998). *J. Appl. Cryst.* **31**, 128–135.
- Ozawa, Y., Terashima, M., Mitsumi, M., Toriumi, K., Yasuda, N., Uekusa, H. & Ohashi, Y. (2003). *Chem. Lett.* **32**, 62–63.
- Paturle, A., Graafsma, H., Sheu, H.-S. & Coppens, P. (1991). *Phys. Rev. B*, **43**, 14683–14691.
- Perman, B., Srajer, V., Ren, Z., Teng, T., Pradervand, C., Ursby, T., Bourgeois, D., Schotte, F., Wulff, M., Kort, R., Hellingwerf, K. & Moffat, K. (1998). *Science*, **279**, 1946–1950.
- Ren, Z., Bourgeois, D., Helliwell, J. R., Moffat, K., Srajer, V. & Stoddard, B. L. (1999). *J. Synchrotron Rad.* **6**, 891–917.
- Rischel, C., Rouse, A., Uschmann, I., Albouy, P.-A., Geindre, J.-P., Audebert, P., Gauthier, J.-C., Forster, E., Martin, J.-L. & Antonetti, A. (1997). *Nature (London)*, **390**, 490–492.
- Rüdlinger, M., Schefer, J., Chevrier, G., Furer, N., Güdel, H. U., Hausühl, S., Heger, G., Schweiss, P., Vogt, T., Woike, T. & Zöllner, H. (1991). *Z. Phys. B Condens. Matter*, **83**, 125–130.
- Rüdlinger, M., Schefer, J., Vogt, T., Woike, T., Hausühl, S. & Zöllner, H. (1992). *Physica (Utrecht) B*, **180/181**, 293–298.
- Sandstrom, D. R., Pyke, S. C. & Lytle, F. W. (1980). Stanford Synchrotron Radiation Laboratory Report 80/01. SSRL, Stanford, CA 94305, USA.
- Sandstrom, D. R., Pyke, S. C. & Lytle, F. W. (1981). Stanford Synchrotron Radiation Laboratory Activities Report, April 1980 to March 1981. SSRL, Stanford, CA 94305, USA.
- Sato, S., Sekine, A., Ohashi, Y., Ishitani, O., Blanco-Rodriguez, A. M., Vlcek, A., Unno, T. & Koike, K. (2007). *Inorg. Chem.* **46**, 3531–3540.
- Schoenlein, R. W., Chattopadhyay, S., Chong, H. H. W., Glover, T. E., Heimann, P. A., Shank, C. V., Zholents, A. A. & Zolotarev, M. S. (2000). *Science*, **287**, 2237.
- Schotte, F., Lim, M., Jackson, T. A., Smirnov, A. V., Soman, J., Olson, J. S., Phillips, G. N., Wulff, M. & Anfinrud, P. A. (2003). *Science*, **300**, 1944–1947.
- Schotte, F., Soman, J., Olson, J. S., Wulff, M. & Anfinrud, P. (2004). *Science*, **147**, 235–246.

- Sekine, A., Tatsuki, H. & Ohashi, Y. (1997). *J. Organomet. Chem.* **536–7**, 389–398.
- Service, R. F. (2002). *Science*, **298**, 1356–1358.
- Spielmann, C., Burnett, N. H., Sartania, S., Koppitsch, R., Schnurer, M., Kan, C., Lenzner, M., Wobrauschek, P. & Krausz, F. (1997). *Science*, **278**, 661–664.
- Stein, P., Dickson, M. K. & Roundhill, D. M. (1983). *J. Am. Chem. Soc.* **105**, 3489–3494.
- Stoermer, M., Andre, J.-M., Michaelsen, C., Benbalagh, R. & Jonnard, P. (2007). *J. Phys. D Appl. Phys.* **40**, 4253–4258.
- Takaoka, K., Kawano, M., Ozeki, T. & Fujita, M. (2006). *Chem. Commun.* pp. 1625–1627.
- Takayama, T., Kawano, M., Uekusa, H., Ohashi, Y. & Sugawara, T. (2003). *Helv. Chim. Acta*, **86**, 1352–1358.
- Techert, S. (2004). *J. Appl. Cryst.* **37**, 445–450.
- Techert, S., Schotte, F. & Wulff, M. (2001). *Phys. Rev. Lett.* **86**, 2030–2033.
- Thiel, D. L., Livins, P., Stern, E. A. & Lewis, A. (1993a). *Nature (London)*, **362**, 40–43.
- Thiel, D. L., Livins, P., Stern, E. A. & Lewis, A. (1993b). *Nature (London)*, **363**, 565.
- Thompson, A. L., Beeby, A. & Goeta, A. E. (2004). *J. Appl. Cryst.* **37**, 652–653.
- Thompson, A. L., Money, V. A., Goeta, A. E. & Howard, J. A. K. (2005). *C. R. Chim.* **8**, 1365–1373.
- Tompkins, R. J., Mercer, I. P., Fettweis, M., Barnett, C. J., Klug, D. R., Porter, Lord, G., Clark, I., Jackson, S., Matousek, P., Parker, A. W. & Towrie, M. (1998). *Rev. Sci. Instrum.* **69**, 3113–3117.
- Vorontsov, I. I. & Coppens, P. (2005). *J. Synchrotron Rad.* **12**, 488–493.
- Vorontsov, I. I., Kovalevsky, A. Y., Chen, Y.-S., Graber, T., Gembicky, M., Novozhilova, I. V., Omary, M. A. & Coppens, P. (2005). *Phys. Rev. Lett.* **94**, 193003.
- Wallace, J. (2006). *Laser Focus World*, Article 257215, <http://www.laserfocusworld.com/resource/photronics> and <http://www.laserfocusworld.com/articles/257215>.
- Weiss, R. G., Ramamurthy, V. & Hammond, G. S. (1993). *Acc. Chem. Res.* **26**, 530–536.
- Wulff, M., Bratos, S., Plech, A., Vuilleumier, R., Mirloup, F., Lorenc, M., Kong, Q. & Ihee, H. (2006). *J. Chem. Phys.* **124**, 034501.
- Yamashita, K. I., Kawano, M. & Fujita, M. (2007). *J. Am. Chem. Soc.* **129**, 1850.
- Yasuda, N., Kanazawa, M., Uekusa, H. & Ohashi, Y. (2002). *Chem. Lett.* **11**, 1132–1133.
- Zheng, S.-L., Messerschmidt, M. & Coppens, P. (2007). *Acta Cryst.* **B63**, 644–649.
- Zimmerman, H. E., Sebek, P. & Zhu, Z. (1998). *J. Am. Chem. Soc.* **120**, 8549–8550.